

Label-Free Mapping of Osteopontin Adsorption to Calcium Oxalate Monohydrate Crystals by Tip-Enhanced Raman Spectroscopy

Nastaran Kazemi-Zanjani,[†] Honghong Chen,[‡] Harvey A. Goldberg,^{‡,§} Graeme K. Hunter,^{‡,§} Bernd Grohe,[‡] and François Lagugné-Labarthe^{*,†}

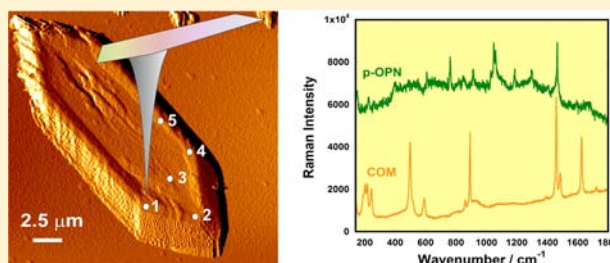
[†]Department of Chemistry, University of Western Ontario (Western University), 1151 Richmond Street, London, Ontario, N6A 5B7, Canada

[‡]School of Dentistry and [§]Department of Biochemistry, Schulich School of Medicine and Dentistry, Western University, London, Ontario, N6A 5C1, Canada

S Supporting Information

ABSTRACT: In the ectopic biomineralization of calcium oxalate kidney stones, the competition between calcium oxalate monohydrate (COM) formation and its inhibition by the phosphoprotein osteopontin (OPN) plays a key role in COM stone-forming processes. To get more insights into these processes, tip-enhanced Raman spectroscopy (TERS) was used to provide surface-specific information about the adsorption of OPN to faces of COM crystals. In TERS, the surface plasmon resonance of a metallic AFM tip is locally excited when the tip is placed in the optical near-field of a laser focused on the crystal surface.

Excitation of this localized surface plasmon resonance allows the enhancement of the Raman signal as well as the improvement of the spatial resolution beyond the diffraction limit of the light. As TERS works label free and noninvasively, it is an excellent technique to study the distribution of adsorbed proteins on crystal faces at the submicrometer scale. In the present work, we generated Raman intensity maps indicating high spatial resolution and a distinct variation in relative peak intensities. The collected TERS spectra show that the OPN preferentially adsorbs to edges and faces at the ends of COM crystals (order: {100}/ {121} edge > {100} face > {100}/ {010} edge ≈ {121}/ {010} edge > {010} face) providing also relevant information on the inhibition of crystal growth. This study demonstrates that TERS is an excellent technique for detailed investigations of biomolecules adsorbed, layered, or assembled to a large variety of surfaces and interfaces.



INTRODUCTION

Tip-enhanced Raman spectroscopy (TERS) is attracting increasing attention across the chemical, biochemical and biophysical sciences.^{1–4} In TERS measurements, a metallized (Au, Ag) Atomic Force Microscopy (AFM) or Scanning Tunneling Microscopy (STM) tip with a tip radius of 10–20 nm is brought in feedback with the surface of a sample.^{5,6} A laser source, aligned and focused to an AFM tip, induces a local resonant excitation of surface plasmons at the metal-coated tip, which in turn provides an enhanced Raman signal of the sample in proximity to the tip apex.⁷ The sample is then scanned point-by-point over a surface providing a TERS map of that surface. The nature of TERS—to be locally very sensitive—can be further evidenced by analyzing the decay rate of the signal magnitude when the tip is brought out of vicinity of the surface of interest. Recently, it has been shown that the intensity of the near-field is inversely proportional to the 10th power of the tip–sample distance.⁸ This feature makes TERS a very valuable technique to specifically probe surfaces and interfaces, and has been used to study individual nanosized building blocks such as carbon nanotubes with a lateral resolution of 15 nm.⁹ This is in sharp contrast to the practical spatial lateral resolution

limit (Δx) of conventional optical microscopy, given by the Abbe's criterion:^{10,11}

$$\Delta x = \frac{0.61\lambda}{NA} \quad (1)$$

where λ is the wavelength of the light source and NA is the numerical aperture of the objective. This leads, under ideal conditions, to a lateral resolution in the range of 250–500 nm.

The use of TERS in the biochemical and biophysical sciences is particularly attractive as, unlike other techniques (e.g., fluorescence spectroscopy and microscopy), it allows for sensitive analyses of very small areas of a sample at a high spatial resolution and in the absence of any label (isotopes, fluorophores etc.). Labeling can lead to undesired artifacts and misinformation, and sometimes requires the synthesis of endogenous fluorophores, which can perturb the native organization of the biosystem of interest.¹²

Using TERS, Deckert and co-workers recently studied individual RNA strands,¹³ isolated mitochondria of yeast cells,¹⁴ various nucleobases¹⁵ and the lipids and protein domains of human cells.¹⁶ For viruses¹⁷ and a malaria-infected cell,¹⁸ they

Received: June 19, 2012

Published: September 19, 2012

found a wealth of structural details (composition and organization) of the proteins located on the cell membrane at the submicrometer scale. Moreover, Meixner et al.¹⁹ investigated monolayers of calf thymus DNA and improved the detection limit to a single DNA strand, opening an innovative spectroscopic technique for the investigation of DNA–drug interactions. In addition, Zenobi et al. have demonstrated that TERS is the method of choice in investigating lipid monolayers on gold surfaces, again emphasizing the nondestructive nature of TERS combined with a spatial resolution better than 50 nm.²⁰

The present work focuses on the use of TERS to study the interactions of the phosphoprotein osteopontin (OPN) with calcium oxalate monohydrate (COM) crystals. The latter is the most common mineral phase of kidney stones ($\approx 75\%$), while OPN is believed to be a potent inhibitor of kidney stone formation.²¹ A perspective view of a COM penetration twin (main habit in physiological environments) is shown in Figure 1.

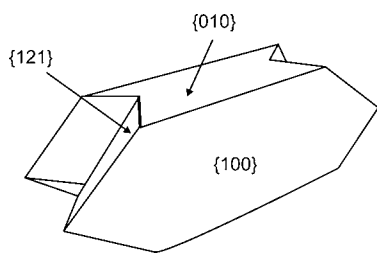


Figure 1. Perspective view of a faceted COM penetration twin depicting the main crystal faces of calcium oxalate monohydrate.

The formation of oxalate stones in the urinary system involves the nucleation, growth, and aggregation of these crystals; a complex process that depends on many parameters such as the diet and water intake of the subject.²² However, low molecular weight (e.g., citrate) and macromolecular inhibitors play an important role in regulating these calcification processes. Members of the latter category are the Tamm–Horsfall protein (THP) and OPN.^{23,24}

OPN, which is part of the body's defense mechanism against pathological calcification,²⁵ is proposed to be a potent inhibitor of stone formation. To test this hypothesis, effects of a variety of OPN peptides and the parent protein on COM growth inhibition were analyzed.^{26–29} In vitro, OPN is adsorbed onto COM crystals,^{22,30,31} inhibits their growth,^{32–34} and prevents crystal aggregation.³⁵ Atomic force microscopy of growth steps, for instance, has shown that OPN adsorption to {010} faces is more selective than adsorption to {100} faces.³⁴ Very recently, the adsorption pattern of OPN isoforms to COM crystals was studied using a combination of confocal fluorescence and scanning electron microscopy.^{28,29,36} These investigations have shown that fluorescent-labeled OPN preferentially adsorbs to the edges between the {100} and {121} faces, and, after longer adsorption times, to {100} faces. Adsorption to {010} and {121} faces was not evident. In the present study, we demonstrate for the first time that a tip-enhanced chemical fingerprint of adsorbed OPN to COM faces results in a detailed, semi-quantitative and complete adsorption profile of the phosphoprotein (phosphorylated recombinant rat bone osteopontin, p-OPN) to COM crystal faces. This is carried out in noncontact mode and without the requirement of fluorescent label. The findings of the present work demonstrate the utility of this novel approach to study protein mineral interactions, and provide important insights into the adsorption behavior of

OPN, which can be used to develop new strategies for therapeutic intervention of pathological calcification.

EXPERIMENTAL SECTION

Chemicals and Solution Preparation. For crystallization of calcium oxalates, reagent grade sodium oxalate ($\text{Na}_2\text{C}_2\text{O}_4$; J. T. Baker), calcium nitrate tetra-hydrate ($\text{Ca}(\text{NO}_3)_2 \cdot 4\text{H}_2\text{O}$; J. T. Baker), sodium chloride (NaCl; J. T. Baker) and sodium acetate (CH_3COONa , anhydrous; Sigma) were used to prepare calcium and oxalate stock solutions as previously described.³⁷ Recombinant full-length rat osteopontin (recOPN) was expressed as an N-terminal His-tagged protein following a protocol used for recombinant bone sialoprotein.³⁸ The purified protein was analyzed by MALDI-TOF mass spectrometry (MALDI-TOF MS; Bruker Reflex III) and a M_w of 36 050 g/mol determined. Phosphorylation of recOPN occurred by treating recOPN with protein kinase CK2 α expressed as a GST-tagged protein following a protocol by Saad et al.³⁹ MALDI-TOF MS revealed that the M_w of phosphorylated recOPN (p-OPN) is 36 694 g/mol. The mass difference between recOPN and p-OPN (644 g/mol) corresponds to 8.05 phosphate groups. To verify identity, protein content and purity, SDS-PAGE and amino acid analysis (Alberta Peptide Institute, Edmonton, Canada) were used. For adsorption experiments, an aqueous stock solution of 2 mg/mL (54.5 μM) p-OPN was prepared.

Crystallization and Adsorption Experiments. COM formation was initiated by modifying a method previously described.²⁸ In brief, a custom-made Teflon block (Figure 2) containing three bottomless

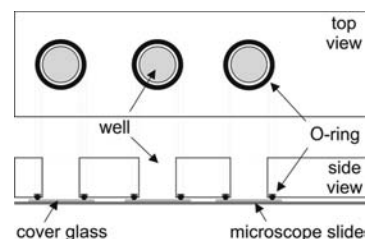


Figure 2. Sketch (not to scale) of a reaction well-containing Teflon block for the growth of COM crystals.

reaction wells (diameter, 9 mm; height, 10 mm) was sealed by o-rings (Viton) with optical cover glass (Fisher, 22 \times 22 mm, No. 1) and clamped using a microscopic slide as bottom cover. Before assembly, the cover glass was treated in 7 wt % NaOH solution at 60 $^\circ\text{C}$ for 20 min to increase negative charge and pit densities of the substrate surfaces in order to have the crystals stick better to the surface of the glass coverslip.^{40–42} This treatment was necessary to prevent crystals from moving during atomic force microscopy scans. All components of the assembly were thoroughly rinsed in doubly distilled H_2O with sonication for 5 min before use.

For crystallization, the reaction assembly and all reaction solutions were preheated to 37 ± 0.2 $^\circ\text{C}$. Thereafter, oxalate solution was added to the wells followed by water and calcium solutions (total volume: 500 μL) and the assembly incubated (Ultra Tec WJ 501 S) at 37 ± 0.2 $^\circ\text{C}$ for 3 h. The final concentrations were $[\text{Ca}^{2+}] = [\text{C}_2\text{O}_4^{2-}] = 1$ mM, sodium acetate 10 mM and sodium chloride 150 mM. For some reactions, pH measurements were carried out immediately after mixing the solutions; the pH was always between 6.65 and 6.75.

For adsorption experiments, crystal growth solutions were exchanged by low-supersaturated calcium oxalate solutions ($[\text{Ca}^{2+}] = [\text{C}_2\text{O}_4^{2-}] = 0.06$ mM, preheated to 37 $^\circ\text{C} \pm 0.2$ $^\circ\text{C}$) followed by the addition of 0.4 mg/mL p-OPN to the wells containing preformed crystals. The total volume was again 500 μL . After allowing adsorption to the crystals for a period of 60 min (37 ± 0.2 $^\circ\text{C}$), cover glass samples were rinsed with deionized water, air-dried and stored in a desiccators until further use.

TERS Setup. The TERS setup was composed of a Raman spectrometer (HR LabRam, Horiba-Jobin-Yvon) connected to an inverted optical microscope (Olympus IX71) and interfaced with an atomic

force microscope (AFM, NanoWizard II Bioscience, JPK Instruments Inc.) to perform measurements in the transmission mode. This 5-axes AFM is equipped with a high resolution piezoelectric x - y sample stage and an x - y - z piezoelectric actuator to independently control the tip position. The linearly polarized coherent laser beam ($\lambda = 532$ nm, Compass 315 M laser) was focused on the sample using an objective with a high numerical aperture (Olympus PlanAPO, N.A. = 0.95, $\times 100$). The same objective was used to collect the backscattered light. The laser intensity at the sample was adjusted to 0.3 mW. The TERS probe was attached to a piezoelectric stage and kept a few nanometers above the sample surface employing a conventional AFM feedback mechanism. AFM scans were conducted in noncontact mode using silver coated AFM tips (NCL20 Nano World Inc.; resonance frequency $f = 170$ kHz, force constant $k = 48$ N/m). Silver coating (30 nm layer) was carried out by electron beam-induced thermal evaporation of the metal. The coated tips were used within a day of coating. Here, 5–10 coated tips were used for each facet, whereas an average of 1 in 5 tips provided large enhancement. At the end of each experiment, a TERS experiment with the tip in proximity to the glass surface was performed to test for a possible contamination of the tip (see Supporting Information: Figure S1)

RESULTS

Raman reference spectra of both the phosphoprotein and the calcium oxalate crystals were acquired (Figure 3). The most

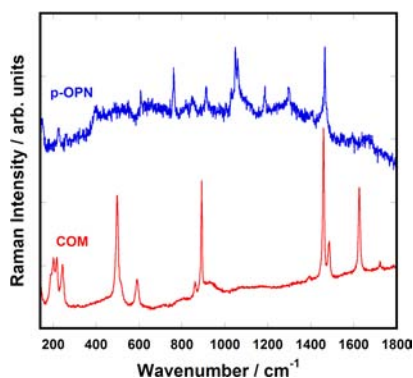


Figure 3. Raman spectra of the phosphoprotein p-OPN and COM crystals. The acquisition times were 120 s for pOPN and 20 s for the COM crystal using similar irradiation conditions. The spectrum of the protein is multiplied by a factor of 10.

intense Raman peak of p-OPN appears at 1465 cm^{-1} which overlaps with a main peak of COM at 1464 cm^{-1} . The presence of OPN can however be distinguished from COM by monitoring the intensity ratio for the wave numbers 1464 cm^{-1} and

1487 cm^{-1} . The latter Raman peak is assigned to COM only. Therefore, the larger the ratio I_{1464}/I_{1487} is, the larger is the amount of proteins adsorbed onto the crystal surface. The peak assignments for both OPN and COM are shown in Table 1.

To investigate the adsorption pattern of OPN on the surface of the COM crystals, we collected TERS maps of both p-OPN adsorbed to $\{100\}$ faces and p-OPN adsorbed to $\{010\}$ faces. The mapping was performed first within selected areas of $10 \times 10\ \mu\text{m}^2$ near the extremities of the crystals. The lateral separation between adjacent pixels inside the mapping region was set to be 250 nm. For each crystal face, collection of Raman signals was carried out sequentially keeping the metallic AFM tip in feedback with the surface of the sample. Prior to scanning, the TERS tip was aligned to the focused excitation beam for each crystal face analyzed. Spectra for maps were acquired using a laser power of 0.3 mW at the sample plane for 1 s. Once all spectra were collected, two sets of maps were generated by integrating the Raman peaks at 1464 cm^{-1} (of COM and p-OPN; Figure 4a,d) and the peaks at 1487 cm^{-1} (of COM only; Figure 4b,e). We then evaluated the p-OPN distribution on the $\{100\}$ and $\{010\}$ crystal faces by calculating the intensity ratios of 1464 and 1487 cm^{-1} peaks for four selected points on each of the two crystal faces. The four points (black dots) are shown in Figure 4a,d, while the spectra and associated ratios are shown in Figure 4c,f.

To clearly demonstrate the TERS effect, Raman spectra were collected at three specific locations on both crystal faces using an acquisition time of 600 s per point (Figure 5). For these measurements, the tip was either kept in the near-field position of the surface (typically 1–10 nm) or in the far-field above the surface ($\sim 1\ \mu\text{m}$). After measurements, TERS spectra were derived by calculating the difference between the Raman spectra acquired in near-field (green color) and the far-field (red color). The near-field and far-field spectra along with the TERS spectra (blue color) of each of these four points are shown in Figure 5. As these TERS spectra represent Raman signals originating from the crystal surface rather than the bulk, they contain a high contribution of signals from the adsorbed p-OPN.

To further investigate the TERS enhancement effect and distribution patterns of p-OPN on surfaces of crystal faces (rather than the edges), we performed mapping of $16 \times 5\ \mu\text{m}^2$ areas on the crystal surface using the conditions described above (acquisition time, 1 s; laser power, 0.3 mW at the crystal surface). For the final maps, integration of the 1464 cm^{-1} peak was carried out. The maps shown in Figure 6 correspond to a region in the middle of the crystal with the tip either in the near-field of the

Table 1. Raman Peak Assignment for p-OPN and COM Crystals

p-OPN (cm^{-1})	COM (cm^{-1})	band intensity	band assignment
	503–595	w	O–C–O bending ⁴³
608		w	C–O bending vibration of amide VI band ⁴⁴
761		m	Indole symmetric breathing mode of Trp, ⁴⁵ Symmetric stretching of O–P–O ⁴⁶
800–900		m	Symmetric C–N–C stretching ⁴⁴
	850–950	m	C–C stretching ⁴³
915		m	C–C stretching of side chains ⁴⁵
1050		s	C–C stretching of side chains ⁴⁵
1062		m	Symmetric P–O stretching vibration, ⁴⁷ C–N stretching of side chains ⁴⁵
1187		w	CO–O–C stretching mode, ⁴⁸ Amide III ⁴⁹
1250–1350		w	Amide III bending and stretching of backbone ⁵⁰
	1300–1500	s	Symmetric C–O stretching ⁴³
1425–1475		s	CH ₂ scissoring or CH ₃ asymmetric stretching ⁵⁰
	1550–1750	m	Asymmetric C–O stretching, ⁴³ Amide I ^{48,51}

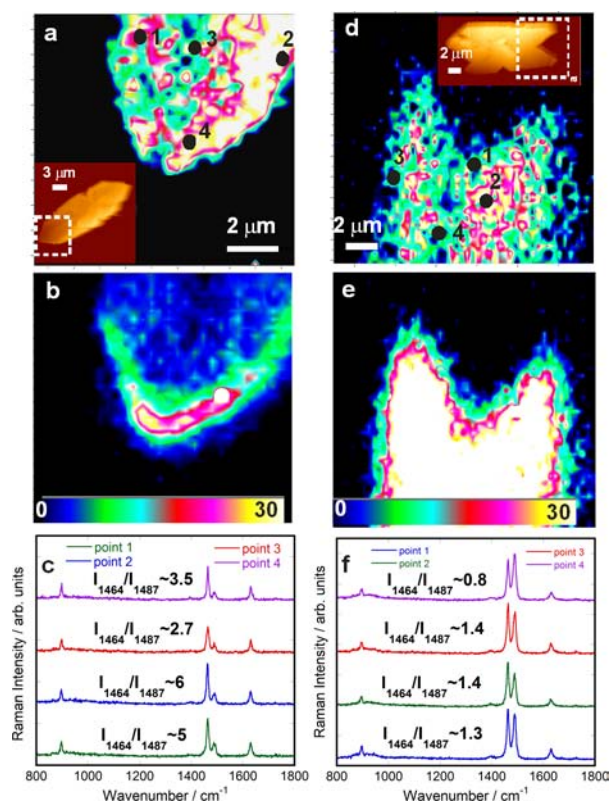


Figure 4. TERS maps of p-OPN adsorbed to $\{100\}$ and $\{010\}$ crystal faces. The color bars represent Raman intensity. Blue and white colors indicate weak and strong Raman signals, respectively. (a and d) Maps resulting from the integration of the OPN-1465 cm^{-1} peak on $\{100\}$ and $\{010\}$ faces (signal of COM and p-OPN), respectively. (b and e) Raman intensity maps resulting from the integration of the 1487 cm^{-1} peak of $\{100\}$ and $\{010\}$ faces (COM only), respectively. (c and f) Raman spectra of four spots (see (a) and (d)) selected from maps on $\{100\}$ and $\{010\}$ faces, respectively.

sample (Figure 6a,c) or in the far-field ($\sim 1 \mu\text{m}$ above the sample; Figure 6b,d).

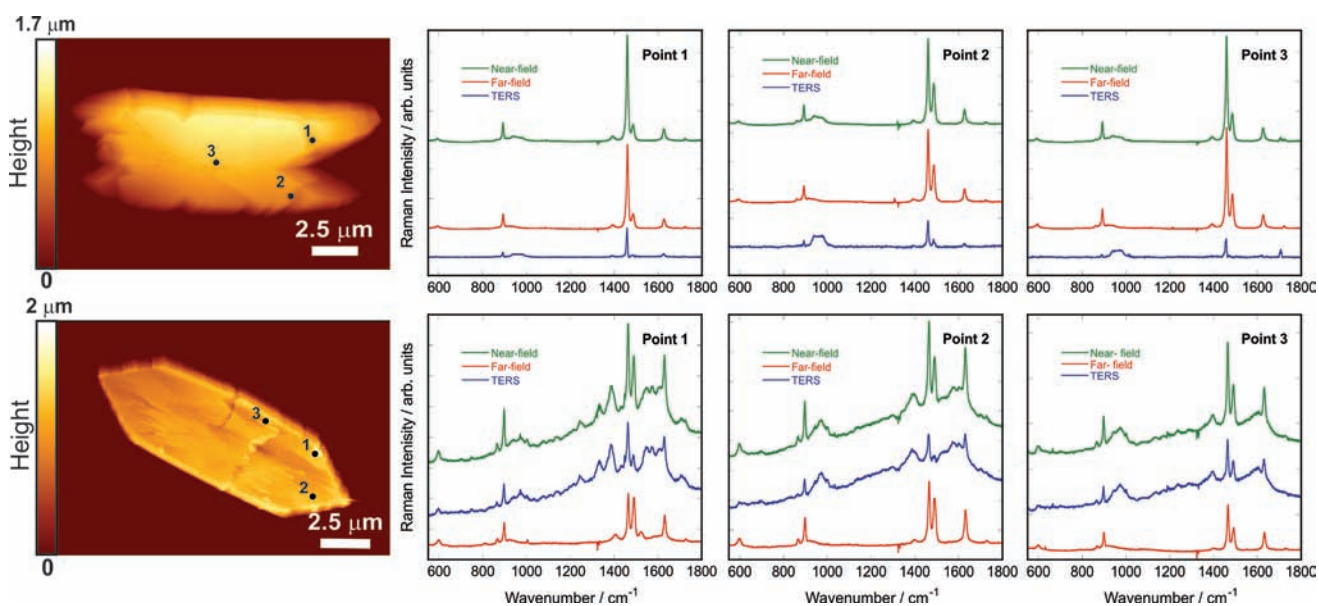


Figure 5. AFM images of (a) $\{010\}$ and (b) $\{100\}$ faces of COM along with Raman spectra (selected spots) of adsorbed p-OPN on COM faces. The green, red, and blue spectra correspond to the near-field, far-field, and TERS spectra, respectively.

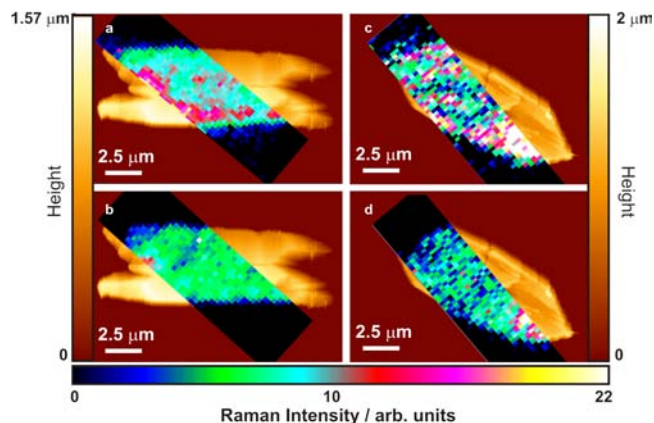


Figure 6. Raman intensity maps of p-OPN adsorbed to an $\{010\}$ face: (a) in TERS, (b) in standard Raman mode. Raman intensity maps of OPN adsorbed to an $\{100\}$ face (c) in TERS and (d) in Raman mode. For both modes, the scanned area was set to be $(20 \times 5) \mu\text{m}^2$, using 330 nm steps along both directions. This results in a total of 900 measuring points.

DISCUSSION

Shown in Figure 4 are the TERS maps and spectra taken from COM $\{100\}$ and $\{010\}$ faces. Each collected signal includes both the near-field contribution from the crystal surface together with the far-field bulk signal from the crystal. Note: TERS of $\{121\}$ faces was not performed, as these faces are not accessible for the tuned AFM/Raman laser setup.

Figure 4a,d shows variations in intensities of the Raman peak at 1464 cm^{-1} for $\{100\}$ and $\{010\}$ faces as well as the crystal edges. Other bands of OPN such as 761 and 1062 cm^{-1} (see Supporting Information: Figures S2–S5) were too weak to be exploited. The measurements indicate the presence of p-OPN and slight changes in thickness of the adsorbed protein layer, which also results in changes of COM intensities. Comparing the TERS spectra of the two maps shown in Figure 4a,d indicates, by variations in intensity, that the phosphoprotein tends to adsorb more to the extremities of the crystal. From

these data, it is apparent that p-OPN adsorbs preferentially to the edges between {100} and {121} faces and, rather marginally, to the {010}/{121} edges. In addition, more intense Raman signals at {100} faces suggest that p-OPN adsorbs more selectively to {100} than to {010} faces. This outcome confirms recent findings by Hunter and co-workers, who report that high Ca^{2+} densities on {100} faces promote the adsorption of the acidic phosphoprotein.^{36,52} Moreover, adsorption of p-OPN to the edges might be an effect of surface energies.^{28,52}

To provide additional evidence for the presence and selectivity of adsorbed p-OPN on COM faces, single spot TERS measurements (four at each crystal face) and calculations of intensity ratios (I_{1464}/I_{1487}) were carried out for each spot. On the {100} face, these ratios were between 2.7 and 6, and for the spots on the {010} face, ratios between 0.4 and 1.4 were calculated (the higher the ratio the higher the OPN concentration, see above). Particularly for the {100} face (Figure 4c), large ratios near the crystal edges were measured (points 1,2,4). For the face itself (point 3), a ratio of 2.7 was received. This value is relatively high compared to those measured for the {010} face (Figure 4f). In addition, the {010}-ratios are more homogeneous and show a lower affinity for p-OPN to {010} faces. In general, the adsorption profile found for p-OPN is in good agreement with results achieved in previous studies using confocal fluorescence microscopy.²⁸ There is, however, one important difference. The semiquantitative results derived in the present study clearly show that p-OPN does not only adsorb relatively strong to {100}/{121} edges, a fact also reported by Taller et al.,²⁸ but also to {100} and (marginally) to {010} faces. In contrast, confocal fluorescence microscopy used by Taller et al. showed very weak (if at all) and undistinguishable binding to {100} and {010} faces.²⁸ Indeed, Hunter et al. have reported slight OPN adsorption to {100} faces but no protein-binding to {010} faces, as well.³⁶ Therefore, using the sensitivity of TERS allowed us to specify the selectivity of OPN adsorption with very high accuracy, finally indicating an order of adsorbed p-OPN of {100}/{121} edges > {100} faces > {010} faces. On the basis of the p-OPN concentration used (0.4 mg/mL) in the present study and the treatment of the samples after adsorption (rinsing the crystals and removing excess of p-OPN [desorption of physisorbed protein]), it is proposed that the p-OPN layers detected by TERS are strongly bound (chemisorbed) protein. In contrast, Taller et al. used very low concentration (1 $\mu\text{g}/\text{mL}$) to study the selectivity (chemisorption) of OPN binding *in situ*.²⁸ Both methods reveal binding affinities to COM edges and faces which are quite comparable, with the obvious difference that TERS is more sensitive. The fact that Hunter et al. found more OPN bound to {100} faces than Taller et al. suggests an effect of the adsorption time.^{28,36} Using the same *in situ* method, Hunter et al. adsorbed for ≥ 90 min, whereas Taller et al. used 60 min, like the present study. It is assumed that these longer treatments applied by Hunter et al. resulted in higher adsorption rates of (physisorbed) OPN to {100} faces.³⁶ Moreover, the adsorption profile found in the present study directly mirrors the growth inhibition profile reported in recent studies.^{28,29,36} These studies indicated strong interactions of the protein with {100}/{121} edges, weaker OPN effects on {100} faces and marginally affected {010} faces when COM was grown in the presence of higher concentrations (5 $\mu\text{g}/\text{mL}$).

Another advantage of TERS (compared to conventional fluorescence microscopy) is the possibility to highly resolve variations in surface roughness, an ability similar to that of AFM (Figure 4b,e). Using the 1487 cm^{-1} peak of COM investigations

indicates that the {010} face shows more homogeneity rather than the {100} face.

Further experiments were performed to estimate the enhancement factor of TERS. To this end, two different sets of spectra were measured: one set (3 spots) in near-field and one set (3 spots) in far-field. Figure 5 clearly shows that a spectrum with higher intensity is obtained (green spectra) when the AFM tip is in near-field position also indicating a higher sensitivity of the near-field mode. The adsorption pattern found by TERS is therefore extractable by performing both near-field and far-field maps. The resulting TERS (blue spectra) is, in turn, the intensity difference between the spectra collected in far-field and in near-field, respectively. This method provides qualitative insights into features of the crystal surface and gives an idea of the tip-enhancement factor.

In the following, we will have a brief look at this effect. An estimation of the enhancement by the TERS effect can be carried out considering two factors. First, the optical contrast between the near-field and far-field, which can be derived by calculating the ratio between the enhanced and nonenhanced contributions.⁷

$$C = \frac{S_{\text{nearfield}}}{S_{\text{farfield}}} \quad (2)$$

In eq. (2), $S_{\text{nearfield}}$ and S_{farfield} are the enhanced and non-enhanced contributions of the Raman signal, respectively. A second factor is the geometrical dimension of the focal point and the AFM tip. Here, the tip diameter and its shape as well as the geometry of the focused beam at the crystal face have to be considered. For the area of the diffraction-limiting focal spot, we can show that

$$A_{\text{farfield}} = r_{\text{laser}}^2 \pi \quad (3)$$

with r_{laser} being the radius of the focused laser.⁷

The area from which the near-field signal is generated can be approximated by:^{7,49}

$$A_{\text{nearfield}} = r_{\text{tip}}^2 \pi \quad (4)$$

where r_{tip} is the radius of the tip. The TERS enhancement factor (EF_{TERS}) can then be calculated according to:

$$\text{EF}_{\text{TERS}} = C \frac{A_{\text{farfield}}}{A_{\text{nearfield}}} \quad (5)$$

Considering a laser spot diameter of 275 nm and a tip diameter of 20 nm, we obtain $A_{\text{farfield}} \sim 0.06 \mu\text{m}^2$ and $A_{\text{nearfield}} \sim 3 \times 10^{-4} \mu\text{m}^2$, respectively. At the best, a contrast factor of $C = 1.5$ (see eq. (2)) can be determined from the difference of intensities between the near-field and the far-field Raman spectra (Figure 5b, points 1–3, peak at 1464 cm^{-1}). This yields to an enhancement factor of $\text{EF} \sim 300$. This value can be compared to enhancement factors reported in the literature for similar TERS experiments, covering a wide range from $\text{EF} = 14$ to 10^8 (using comparable setups and experimental conditions, but different samples).^{9,19,49,53}

The TERS spectra shown in Figure 5a for points 1–3 are weaker compared to the spectra (points 1–3) shown in Figure 5b. This is caused by a smaller enhancement factor for signals taken at {010} and confirms again the preference of OPN for the {100} face. Figure 5b shows that the TERS signal measured in Point 1 (located at the edge between {100} and {121} faces) is the most intense, suggesting a high affinity of OPN to these edges.

Intensity maps of larger areas were measured in near- and far-field (Figure 6) to get more information about the overall

distribution of p-OPN adsorbed to crystal faces. In general, these maps validate the results and data described above (Figure 4). It is, however, important to note that OPN also shows tendencies to adsorb to the edges between {100} and {010} faces of COM (Figure 6a,c), a result not detected in previous fluorescence studies.

CONCLUSIONS

In summary, we have demonstrated for the first time that tip-enhanced Raman spectroscopy can provide valuable insights into the adsorption behavior of OPN on calcium oxalate monohydrate crystals without any need to label the protein. Despite the fact that some factors such as the quality of the metal coating of the TERS tip can influence the spatial resolution of this technique, our findings provide valuable insights into the adsorption pattern of the phosphoprotein to COM crystal faces. On the basis of the results of this study, OPN tends to adsorb preferentially to {100}/{121} edges at the ends of the crystal and, less preferentially, to {100} faces. We also observed some adsorption to {010}/{121} and {100}/{010} edges. The final adsorption pattern found shows the preference: {100}/{121} edge > {100} face > {100}/{010} edge \approx {121}/{010} edge > {010} face. The fact that the {100} face exhibited more adsorbed OPN than the {010} face is presumably related to the higher Ca^{2+} ions density on the {100} face. Adsorption to the edges might be a result of higher surface energies in these regions. In general, it was shown that TERS is a label-free, highly sensitive and noninvasive technique, which is able to show detailed information of the adsorption pattern of proteins, a method also useful for studying other systems such as self-assembled, layered or arrayed structures.

Abbreviations. AFM, Atomic Force Microscopy; STM, Scanning Tunneling Microscopy; COM, Calcium Oxalate Monohydrate; p-OPN, phosphorylated recombinant osteopontin; MALDI-TOF, Matrix Assisted Laser Desorption/Ionization linear time of flight spectroscopy; TERS, Tip-Enhanced Raman Spectroscopy; s, strong; w, weak; m, medium.

ASSOCIATED CONTENT

Supporting Information

Figures S1–S5. This material is available free of charge via the Internet at <http://pubs.acs.org>.

AUTHOR INFORMATION

Corresponding Author

flagugne@uwo.ca

Notes

The authors declare no competing financial interest.

ACKNOWLEDGMENTS

The authors gratefully acknowledge the Nanofabrication Facility at Western University for the preparation of the TERS probes. This research was funded by the Natural Sciences and Engineering Research Council of Canada and by the Canadian Institutes of Health Research.

REFERENCES

- (1) Domke, K. F.; Zhang, D.; Pettinger, B. *J. Am. Chem. Soc.* **2007**, *129*, 6708.
- (2) Domke, K. F.; Pettinger, B. *ChemPhysChem* **2010**, *11*, 1365.
- (3) Deckert-Gaudig, T.; Kammer, E.; Deckert, V. *J. Biophotonics* **2012**, *5*, 215.

- (4) Hartschuh, A.; Qian, H.; Meixner, A. J.; Anderson, N.; Novotny, L. *Surf. Interface Anal.* **2006**, *38*, 1472.
- (5) Novotny, L. *Nature* **2008**, *455*, 887.
- (6) Novotny, L.; van Hulst, N. *Nat. Photonics* **2011**, *5*, 83.
- (7) Stadler, J.; Schmid, T.; Zenobi, R. *Nanoscale* **2012**, *4*, 1856.
- (8) Cañado, L. G.; Jorio, A.; Ismach, A.; Joselevich, E.; Hartschuh, A.; Novotny, L. *Phys. Rev. Lett.* **2009**, *103*, 186101/1.
- (9) Cañado, L. G.; Hartschuh, A.; Novotny, L. *J. Raman Spectrosc.* **2009**, *40*, 1420.
- (10) Novotny, L.; Hetch, B. *Principles of Nano-Optics*; Cambridge University Press: New-York, NY, 2006.
- (11) Hartschuh, A.; Sanchez, E. J.; Xie, X. S.; Novotny, L. *Phys. Rev. Lett.* **2003**, *90*, 095503/1.
- (12) Deckert-Gaudig, T.; Deckert, V. *Phys. Chem. Chem. Phys.* **2010**, *12*, 12040.
- (13) Bailo, E.; Deckert, V. *Angew. Chem., Int. Ed.* **2008**, *47*, 1658.
- (14) Böehme, R.; Mkandawire, M.; Krause-Buchholz, U.; Rösch, P.; Roedel, G.; Popp, J.; Deckert, V. *Chem. Commun. (Cambridge, U.K.)* **2010**, *47*, 11453.
- (15) Treffer, R.; Bailo, E.; Deckert-Gaudig, T.; Deckert, V. *Beilstein J. Nanotechnol.* **2011**, *2*, 628.
- (16) Richter, M.; Hedegaard, M.; Deckert-Gaudig, T.; Lampen, P.; Deckert, V. *Small* **2011**, *7*, 209.
- (17) Cialla, D.; Deckert-Gaudig, T.; Budich, C.; Laue, M.; Moeller, R.; Naumann, D.; Deckert, V.; Popp, J. *J. Raman Spectrosc.* **2009**, *40*, 240.
- (18) Wood, B. R.; Bailo, E.; Khiavi Mehdi, A.; Tilley, L.; Deed, S.; Deckert-Gaudig, T.; McNaughton, D.; Deckert, V. *Nano Lett.* **2011**, *11*, 1868.
- (19) Hennemann, L. E.; Meixner, A. J.; Zhang, D. *Spectroscopy (Amsterdam, Neth.)* **2010**, *24*, 119.
- (20) Opilik, L.; Bauer, T.; Schmid, T.; Stadler, J.; Zenobi, R. *Phys. Chem. Chem. Phys.* **2011**, *13*, 9978.
- (21) Bushinsky, D. A. *Adv. Intern. Med.* **2001**, *47*, 219.
- (22) Khan, S. R.; Kok, D. J. *Front. Biosci.* **2004**, *9*, 1450.
- (23) Giachelli, C. M. *Orthod. Craniofac. Res.* **2005**, *8*, 229.
- (24) Kumar, V.; Lieske, J. C. *Curr. Opin. Nephrol. Hypertens.* **2006**, *15*, 374.
- (25) Kleinman, J. G.; Wesson, J. A.; Hughes, J. *Nephron* **2004**, *98*, 43.
- (26) Grohe, B.; O'Young, J.; Ionescu, D. A.; Lajoie, G.; Rogers, K. A.; Karttunen, M.; Goldberg, H. A.; Hunter, G. K. *J. Am. Chem. Soc.* **2007**, *129*, 14946.
- (27) Hug, S.; Grohe, B.; Jalkanen, J.; Chan, B.; C., G. B.; Vincent, K.; Lagugné-Labarthe, F.; Lajoie, G.; Goldberg, H. A.; Karttunen, M.; Hunter, G. K. *Soft Matter* **2012**, *8*, 1226.
- (28) Taller, A.; Grohe, B.; Rogers, K. A.; Goldberg, H. A.; Hunter, G. K. *Biophys. J.* **2007**, *93*, 1768.
- (29) Grohe, B.; Taller, A.; Vincent, P. L.; Tieu, L. D.; Rogers, K. A.; Heiss, A.; Sorensen, E. S.; Mittler, S.; Goldberg, H. A.; Hunter, G. K. *Langmuir* **2009**, *25*, 11635.
- (30) Kok, D. J. *World J. Urol.* **1997**, *15*, 219.
- (31) Wesson, J. A.; Worcester, E. M.; Wiessner, J. H.; Mandel, N. S.; Kleinman, J. G. *Kidney Int.* **1998**, *53*, 952.
- (32) Shiraga, H.; Min, W.; VanDusen, W. J.; Clayman, M. D.; Miner, D.; Terrell, C. H.; Sherbotie, J. R.; Foreman, J. W.; Przysiecki, C.; Neilson, E. G.; Hoyer, J. R. *Proc. Natl. Acad. Sci. U.S.A.* **1992**, *89*, 426.
- (33) Worcester, E. M.; Blumenthal, S. S.; Beshensky, A. M.; Lewand, D. L. *J. Bone Miner. Res.* **1992**, *7*, 1029.
- (34) Qiu, S. R.; Wierzbicki, A.; Orme, C. A.; Cody, A. M.; Hoyer, J. R.; Nancollas, G. H.; Zepeda, S.; De Yoreo, J. J. *Proc. Natl. Acad. Sci. U.S.A.* **2004**, *101*, 1811.
- (35) Wesson, J. A.; Ganne, V.; Beshensky, A. M.; Kleinman, J. G. *Urol. Res.* **2005**, *33*, 206.
- (36) Hunter, G. K.; Grohe, B.; Jeffrey, S.; O'Young, J.; Sorensen, E. S.; Goldberg, H. A. *Cells Tissues Organs* **2009**, *189*, 44.
- (37) Grohe, B.; Rogers, K. A.; Goldberg, H. A.; Hunter, G. K. *J. Cryst. Growth* **2006**, *295*, 148.
- (38) Tye, C. E.; Hunter, G. K.; Goldberg, H. A. *J. Biol. Chem.* **2005**, *280*, 13487.

- (39) Saad, F. A.; Salih, E.; Wunderlich, L.; Flueckiger, R.; Glimcher, M. J. *Biochem. Biophys. Res. Commun.* **2005**, *333*, 443.
- (40) Meyer, P.; Jouffroy, M.; Membrey, F.; Fromm, M.; Chambaudet, A. *Radiat. Prot. Dosim.* **1997**, *74*, 75.
- (41) Behrens, S. H.; Grier, D. G. *J. Chem. Phys.* **2001**, *115*, 6716.
- (42) Mellott, N. P.; Brantley, S. L.; Hamilton, J. P.; Pantano, C. G. *Surf. Interface Anal.* **2001**, *31*, 362.
- (43) Frost, R. L.; Weier, M. L. *Thermochim. Acta* **2004**, *409*, 79.
- (44) Socrates, G. *Infrared and Raman Characteristic Group Frequencies: Tables and Charts*, 3rd ed.; Wiley: Chichester, 2004.
- (45) Stewart, S.; Fredericks, P. M. *Spectrochim. Acta, Part A* **1999**, *55A*, 1615.
- (46) Hermann, P.; Fabian, H.; Naumann, D.; Hermelink, A. *J. Phys. Chem. C* **2011**, *115*, 24512.
- (47) Zhang, D.; Ortiz, C.; Xie, Y.; Davisson, V. J.; Ben-Amotz, D. *Spectrochim. Acta, Part A* **2005**, *61A*, 471.
- (48) Böehme, R.; Richter, M.; Cialla, D.; Rösch, P.; Deckert, V.; Popp, J. *J. Raman Spectrosc.* **2009**, *40*, 1452.
- (49) Budich, C.; Neugebauer, U.; Popp, J.; Deckert, V. *J. Microsc. (Oxford, U.K.)* **2008**, *229*, 533.
- (50) Matthaus, C.; Chernenko, T.; Newmark, J. A.; Warner, C. M.; Diem, M. *Biophys. J.* **2007**, *93*, 668.
- (51) Kurouski, D.; Deckert-Gaudig, T.; Deckert, V.; Lednev, I. K. *J. Am. Chem. Soc.* **2012**, *134*, 13323.
- (52) Grohe, B.; Hug, S.; Langdon, A.; Jalkanen, J.; Rogers, K. A.; Goldberg, H. A.; Karttunen, M.; Hunter, G. K. *Langmuir* **2012**, *28*, 12182.
- (53) Pettinger, B.; Ren, B.; Picardi, G.; Schuster, R.; Ertl, G. *Phys. Rev. Lett.* **2004**, *92*, 0961011.